Smart Structures and Systems, *Vol. 33, No. 6 (2024) 415-430*
https://doi.org/10.12989/sss.2024.33.6.415

Pedestrian- and wind-induced bi-directional compound vibration control using multiple adaptive-passive TMD-TLD system

Liangkun Wang [1,2a], Ying Zhou*[1,2] and Weixing Shi [1,2b]

[1] *State Key Laboratory of Disaster Reduction in Civil Engineering, Tongji University, Shanghai, 200092, P.R. China*
[2] *Department of Disaster Mitigation for Structures, Tongji University, Shanghai, 200092, P.R. China*

(*Received August 18, 2023, Revised February 6, 2024, Accepted August 5, 2024*)

Abstract. To control vertical and lateral compound vibration simultaneously using an integrated smart controller, passive tuned mass damper (TMD) and tuned liquid damper (TLD) are updated and combined to an adaptive-passive TMD-TLD (AP-TMD-TLD) system. As for the vertical AP-TMD part on top of the vertical spring, it can retune itself through varying the level of liquid in the tank to adjust its mass, while the lateral AP-TLD part at the bottom of the vertical spring can retune itself by changing the level of liquid. Further, for multimodal response control, the multiple AP-TMD-TLD (MAP-TMD-TLD) system is proposed as well. Each AP-TMD-TLD in the system can identify the structural vertical and lateral modal frequencies through the wavelet-transform (WT) based algorithm and retune its vertical and lateral natural frequencies both through adjusting the level of liquid in the AP-TMD and AP-TLD parts respectively. A cantilever cable-stayed landscape bridge which is sensitive to both human-induced and wind-induced vibrations is presented as a case study. For comparison, initial parameters of MAP-TMD-TLD are mistuned. Results show that the presented system can retune its vertical and lateral frequencies precisely, while the retuned system has a better bi-directional compound control effect than the mistuned system before the retuning operation and can improve the serviceability significantly.

Keywords: adaptive tuned liquid damper; cantilever cable-stayed landscape bridge; human-induced vibration; multiple tuned mass damper; serviceability problem; wind-induced vibration

1. Introduction

Benefit from the improvement of design and construction level, long-span steel structures are more and more common in cities. However, because of the lightweight structural form and low damping ratio, it suffers from external excitations and the serviceability problem will be caused when the resonance occurs. Lots of research can be found which are focused on the serviceability problem, and they can be divided into three areas generally, which are human-induced vertical vibration (Cao and Chen 2020, Moutinho *et al*. 2018), human-induced lateral vibration (Bocian *et al*. 2015, Brownjohn *et al*. 2018, Ingolfsson *et al*. 2012, Jiménez-Alonso *et al*. 2019, Racic and Brownjohn 2012) and wind-induced lateral vibration (Wang *et al*. 2021c) respectively.

The tuned mass damper (TMD) is one of the most traditional and popular mechanical vibrational absorbers for structural serviceability improvement (Spencer and Nagarajaiah 2003, Wang *et al*. 2023). When a TMD is well-tuned, it can control the vibration effectively, and dissipate the kinetic energy through its damping element (Nagarajaiah 2010, Wang *et al*. 2020b). TMD has a wide range of application in human-induced vibration control. As for the vertical direction, Casado *et al*. (2013) proposed passive and active TMDs for an in-service pedestrian bridge. Moutinho *et al*. (2018) used passive and semi-active TMDs to control the vibration of a slender footbridge. Zhu *et al*. (2019) presented a combined method to control human-induced vibrations in bridges. As for the lateral direction, Ferreira and Simões (2019) proposed a least cost design of cable-stayed pedestrian bridges with TMDs. Ferreira *et al*. (2019) presented a semi-active TMD for synchronous lateral human-induced vibration control in bridges. Jiménez-Alonso and Sáez (2018) proposed a motion-based design of TMD considering uncertainty conditions. It can be known from the literature review in this paragraph that a well-tuned TMD has a satisfactory human-induced vibration control effect both in vertical and lateral directions.

In addition to the above human-induced vibration control function, TMD can control wind-induced lateral vibration as well (Xing *et al*. 2022, Khazaali *et al*. 2024). Acosta *et al*. (2022) used a TMD for a building to control peak floor accelerations. Lalonde *et al*. (2020) compared the wind-induced vibration control effect of semi-active and passive TMDs for a wind turbine. Nagarajaiah and Varadarajan (2005) proposed a short time Fourier transform (STFT) based semi-active TMD for a wind-sensitive benchmark tall building, while Wang *et al*. (2024) presented an adaptive-passive eddy current pendulum TMD for it. Zuo *et al*. (2020) proposed a TMD for an offshore monopile

*Corresponding author, Ph.D., Professor,
E-mail: yingzhou@tongji.edu.cn
[a] Assistant Professor, E-mail: wangliangkun@tongji.edu.cn
[b] Professor, E-mail: swxtgk@tongji.edu.cn

ISSN: 1738-1584 (Print), 1738-1991 (Online)

wind turbine, while Liu *et al*. (2020a) presented a tiny eddy current TMD for a cylinder solar tower. Though a well-tuned TMD can control wind-induced vibration effectively, a single TMD only has one constant control mode. A multiple TMD (MTMD) system consists of several TMDs with different frequencies (Nagarajaiah and Sonmez 2007), and therefore is more robust (Wang *et al*. 2020c). However, a passive TMD is sensitive to the frequency deviation between the structural natural frequency and itself (Sun *et al*. 2014), a mistuned TMD will lose its control effect (Sun and Nagarajaiah 2014, Liu *et al*. 2020b, Wang *et al*. 2024).

As well as the above TMD, tuned liquid damper (TLD) is also a practical lateral vibration controller. TLD uses the side force generated by the liquid in the stationary tank during sloshing to provide the damping effect. It has the advantages of simple detail, easy installation, good automatic activation performance, no need for starting device, etc., and can be used as water supply tank as well. Shad *et al*. (2016) investigated the efficiency of TLD under harmonic excitations. Shad *et al*. (2018) proposed an experiment on TLDs with an upper mounted baffle. Zahrai and Kakouei (2019) proposed a shaking table test on cylindrical and rectangular TLDs with rotatable baffles. However, the same as TMD, a passive TLD is also a frequency-dependent damper and lacks the adaptability.

The steel cantilever cable-stayed landscape bridge is a kind of special bridge. Usually, it is above the lake for pedestrians to go sightseeing. Because of the slender shape and low damping ratio, it is sensitive to both human-induced vibration and wind-induced vibration. Hoa *et al*. (2020) proposed a model updating method for a large-scale cable-stayed bridge. Larsen and Larose (2015) investigated dynamic characteristics of suspension and cable-stayed bridges under wind-induced excitations. Lazzari *et al*. (2019) analyzed the constructive steps of it. Qian *et al*. (2022) proposed a static instability study for a super-long-span cable-stayed bridge. Raeesi *et al*. (2019) presented a 3D aeroelastic model for it in unsteady wind conditions. Kontoni and Farghaly (2019) used TMDs to control the cable-stayed bridge under earthquake excitations.

It can be known from the above literature review that most references are focused on the serviceability problem which is only caused by one kind of external excitation, whether human-induced vertical/lateral vibration or wind-induced lateral vibration. However, for a complex structure, such as the mentioned cantilever cable-stayed landscape bridge, it may be sensitive to the above excitations simultaneously. Nevertheless, there is a lack of research on smart integrated devices that can control the vertical and lateral bi-directional compound vibration at the same time.

Recently, the authors proposed an adaptive TMD with variable mass for vertical human-induced vibration control (Wang *et al*. 2020a, 2021a), whose mass was composed by a water tank, which could retune itself through varying the level of liquid in the tank to adjust its mass. Meanwhile, considering the frequency of TLD is also depended on the level of liquid, to control vertical and lateral compound vibration simultaneously using an integrated smart controller, a combined adaptive-passive TMD-TLD (AP-TMD-TLD) system is proposed in this study. For multimodal response control, the multiple AP-TMD-TLD (MAP-TMD-TLD) system is presented further. Recently, a two-dimensional air spring based semi-active TMD was proposed by Wang *et al*. (2021c), however, compared to the AP-TMD-TLD in this study, their mechanical models and working mechanisms are different, and multimodal response control was absent in this reference.

The electromechanical model and working mechanism of AP-TMD-TLD and MAP-TMD-TLD are shown in section 2. Then, a large-scale steel cantilever cable-stayed landscape bridge is presented as a case study, and retuning results of the MAP-TMD-TLD system are also proposed in section 3. Finite element analysis results of human-induced vibration control, wind-induced vibration control and their bi-directional compound vibration control are proposed in section 4~6 respectively. Finally, conclusions are drawn in section 7.

2. Electromechanical detail and working mechanism of MAP-TMD-TLD

2.1 Electromechanical model

To control human- and wind-induced vertical and lateral bi-directional compound vibration simultaneously, a combined adaptive-passive TMD-TLD (AP-TMD-TLD) is proposed in Fig. 1.

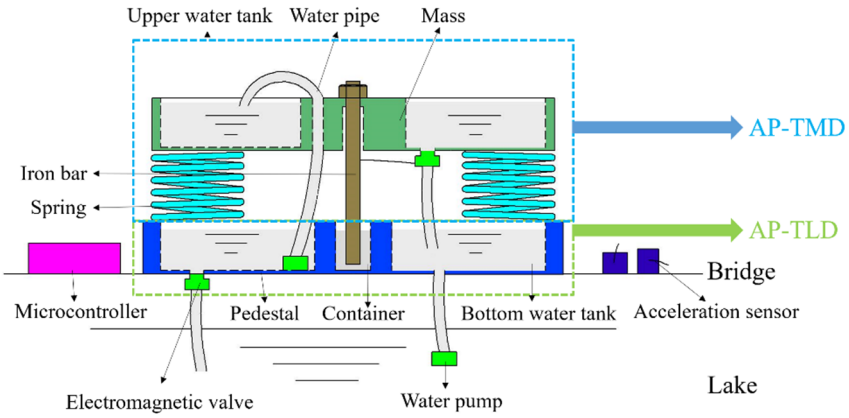

Fig. 1 Schematic diagram of AP-TMD-TLD

In Fig. 1, the AP-TMD-TLD consists of two parts, which are AP-TMD part on top of the vertical spring for vertical vibration control, and lateral AP-TLD part at the bottom of the vertical spring for lateral vibration control respectively. The basic idea is to vary the level of liquid in the upper water tank to adjust the mass and therefore the frequency of AP-TMD part. Meanwhile, the frequency of AP-TLD part can be retuned by changing the level of liquid in the bottom water tank as well.

For a cantilever cable-stayed landscape bridge over a lake, water can be easily obtained and discharged. Therefore, in Fig. 1, as for the AP-TMD part, water in the upper tank can flow into the bottom tank through the electromagnetic valve plugs into the lower surface of the upper tank, to reduce the mass and increase the frequency; inversely, water in the bottom tank can be pumped into the upper tank through the water pump in the bottom tank, to increase the mass and decrease the frequency. As for the AP-TLD part, water in the bottom tank can flow into the lake through the electromagnetic valve plugs into the pedestal, to lower the liquid level and decrease the frequency; inversely, a pump in the lake can pump the water into the bottom tank, to increase the liquid level and therefore the frequency. It also can be seen that the AP-TLD part can not only adjust the liquid level in the vertical AP-TMD part, but also control the lateral vibration independently. The liquid level in the AP-TLD is the result of the interaction between the upper AP-TMD and lake water.

The damping of the AP-TMD part is provided by the vertical relative motion between the iron bar and silicone oil in the container. The damping of the AP-TLD part is provided by the liquid itself or additional details (Shad *et al*. 2018, Zahrai and Kakouei 2019).

Vertical and lateral acceleration sensors installed on the bridge are used to collect its bi-directional dynamic responses under ambient excitation. After the acceleration signal is collected by the microcontroller, the frequency retuning function of AP-TMD-TLD is carried out according to the control algorithm based on wavelet transform (WT) as will be introduced in section 2.3.

In practical engineering applications, the AP-TMD-TLD can be placed under the bridge panels and bolted to the steel beams to avoid impact on pedestrian traffic. Because the adaptive control requires very little power, the battery can be used to power the control system, and the battery can be replaced during regular maintenance of the system. The top AP-TMD works as TMD and controls the vertical vibration, while the bottom part works as TLD and controls the horizontal vibration. To avoid the horizontal direction influence of the top part, in real applications, there will be several horizontal and vertical screens in the top part, at the same time play the role of reducing liquid volatilization.

2.2 MAP-TMD-TLD

The proposed AP-TMD-TLD in the previous section can control the vertical and lateral compound vibration. However, it is still a single mode controller. For multimodal response control of complex structures, the multiple AP-TMD-TLD (MAP-TMD-TLD) system is necessary. For each AP-TMD-TLD in the MAP-TMD-TLD system, it can identify structural vertical and lateral modal frequencies where it located through the WT - based algorithm, and then, retune its vertical and lateral natural frequencies both through adjusting the level of liquid in the AP-TMD part and AP-TLD part respectively, as proposed in the previous section.

The distribution of MAP-TMD-TLD can be determined according to the modal shape of the structure. Usually, a better control effect can be achieved by placing each AP-TMD-TLD in the MAP-TMD-TLD system where structural modal response is the greatest accordingly. There can be an error between the analysis result of finite element model and real structure, and the frequency change will occur in the normal use of the structure as well, both will result in a mistuned passive TMD/TLD. The MAP-TMD-TLD system can be regarded as a combined passive M-TMD-TLD system with an adaptive frequency retuning device. After the mentioned retuning operation, it works the same as a passive damper system, with a reasonable frequency distribution. Therefore, it can solve the vibration problem of complex structure with close modes affected by multiple modal responses with a better effect.

2.3 Variable frequency control mechanism

With a frequency retuning mechanical detail as shown in Fig. 1, a key technical point for the AP-TMD-TLD is the identification of structural dominant modal frequency. A wavelet transform (WT) based control algorithm is introduced in this section.

WT is widely used in non-stationary signal processing and has the characteristics of multi-resolution analysis. WT can refine the vibration signal of the structure through the telescopic translation operation, and achieve the effect of better time resolution in the high frequency domain and better frequency resolution in the low frequency domain. Therefore, WT can be well adapted to the requirements of time-frequency signal analysis. When it is time to retune the MAP-TMD-TLD system, under ambient excitation, for each AP-TMD-TLD, the microcontroller will receive the vertical/lateral acceleration signal from the according acceleration sensor for a pre-set time. Then, for each time segment broken by WT, the dominant frequency with the highest power spectra density can be obtained, and the final identified result is the mean of them. Detailed information about the WT - based algorithm can be referred to Wang *et al*. (2024).

Continuous wavelet transform (CWT) is used in this paper while the Morlet wavelet function is adopted. Morlet wavelet function is widely used in signal analysis. It has good time domain local property and high resolution. It is a kind of wavelet function with fixed frequency, which is obtained by combining the Gaussian distribution function with the cosine function. The local concentration of the Morlet wavelet function in time domain and frequency domain is very high, and the oscillation and amplitude change characteristics in a certain time period can be relatively accurately captured, which is very important for

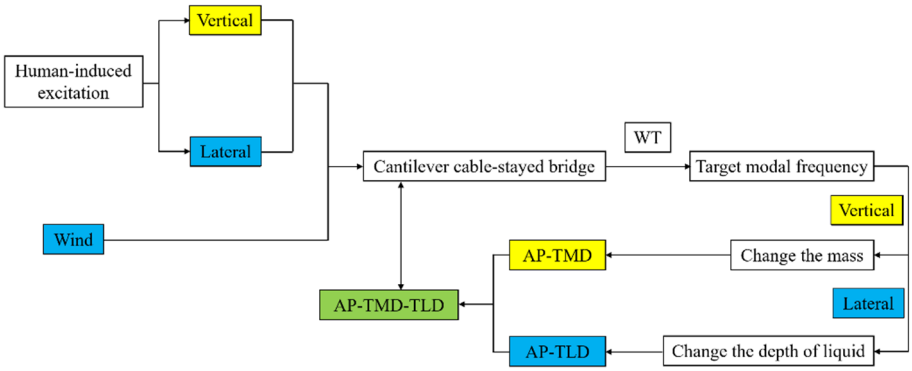

Fig. 2 The combined variable frequency working mechanism of AP-TMD-TLD

signal processing. The bandwidth in the frequency domain is very narrow, so it has a high frequency resolution. It has symmetry in the time domain, but not in the frequency domain, which makes it better to deal with real signals. Its center frequency can be adjusted, so different center frequencies can be used to analyze signals in different frequency bands, which makes it adaptable and flexible.

As for the AP-TMD part in Fig. 1, the mass is adjusted according to the identified vertical structural modal frequency. As for the AP-TLD part, the deep-water TLD model is adopted in this study (Shad *et al*. 2018). Therefore, only the first-order sloshing mode of TLD water body is considered. According to the classical potential flow theory, water body is assumed to be ideal incompressible non-viscous fluid. The water body fluctuates slowly without rotation. The container wall is rigid and there is no friction and adhesion between water body. For a deep-water TLD, the above assumptions are applicable in the case of human-induced vibration control and wind-induced vibration control because the liquid is deep and the sloshing amplitude is small relatively. The sloshing circular frequency of TLD ω_{TLD} is shown as following (Zahrai and Kakouei 2019).

$$\omega_{TLD} = \sqrt{\frac{\pi g}{a} tanh\left(\frac{\pi h}{a}\right)} \tag{1}$$

where a and h are the length and liquid level of TLD respectively. Note that the length direction of TLD is its vibrational direction.

Therefore, according to Equation (1), as for the AP-TLD part in Fig. 1, the liquid level is changed according to the identified lateral structural modal frequency. The combined variable frequency working mechanism of AP-TMD-TLD is proposed in Fig. 2.

In the serviceability problem, the structure can hardly have a sudden frequency change, while the AP-TMD-TLD is focused on the structural natural frequency retuning but not the instantaneous vibrational frequency. Therefore, it is suggested that a monthly retuning operation is enough, while during the retuning operation, it will be better if the structure is only under ambient excitation. It can be easily achieved because the retuning operation only takes about one minute as will be shown in the next section. Hence, it can retune itself during installation for the structure and during normal use of the structure, further, it can be updated to a semi-active controller which can be retuned in real time easily.

In the MAP-TMD-TLD system, some AP-TMD-TLDs distributed on different locations are focused on the same structural target mode frequency, while others are focused on another dominant mode frequency. It is well-known that different AP-TMD-TLDs targeted at different structural modal frequencies will lead to significantly different identification results. However, AP-TMD-TLDs targeted at the same structural modal frequency can have a slightly different identification result as well, because they are distributed at different locations.

When the AP-TMD-TLD is targeted at the same structural modal frequency, its different location on the bridge will cause a slight difference in the identification result. The presence of AP-TMD-TLD will affect the identification of structural natural frequency at its location, and the influence degree of AP-TMD-TLD with different parameters is different as well. In addition, the identification method proposed in this paper is an approximate identification of the structural modal frequency coupled with the dynamic vibration absorber. Therefore, although for the same structural modal frequency, the identification results of AP-TMD-TLD at different locations will be slightly different.

TMD and TLD are both typical frequency-dependent dynamic vibration absorber, their control effect depends on the well-tuned frequency. Therefore, in this paper, the frequency retuning criteria of the AP-TMD-TLD system is that AP-TMD and AP-TLD are both retuned to the identified structural target mode frequency. Then, the liquid level in the top part of AP-TMD is retuned as well as its mass and frequency; the liquid level in the bottom part of AP-TLD is retuned as well as its frequency. After retuning the liquid level in both AP-TMD and AP-TLD parts, the AP-TMD-TLD and then the whole MAP-TMD-TLD system becomes a new passive integrated control system with a reasonable frequency distribution.

3. Case study and retuning simulation

3.1 Cantilever cable-stayed landscape bridge

A steel cantilever cable-stayed landscape bridge which

is sensitive to both human-induced vertical/lateral vibration and wind-induced vibration is presented as a case study, and is shown in Fig. 3. The finite element model is built in MIDAS/Gen.

In Fig. 3, the width of the walkway on both sides of the landscape bridge is 1.8 m, the height is also 1.8 m, and the bottom elevation is 9.0 m. The height of the towers on both sides is 26 m. The left side of the tower and the fixed end are connected by 6 cables, while its right side and the cantilever end of the bridge are connected by 3 groups of cables, each group of 2 cables, and the diameter of the cables is 3 cm. The vibration of the landscape bridge is mainly concentrated in the cantilever ends in the right of the two towers, whose dimensions and overall coordinate system are presented in Fig. 3(b), and A~J are recorded as measuring points.

Through modal analysis, modal information of the cantilever cable-stayed landscape bridge is proposed in Table 1.

Table 1 Modal information of the cantilever cable-stayed landscape bridge

Mode	Frequency (Hz)	Modal mass participation coefficient (%)		
		X-direction	Y-direction	Z-direction
1	0.62	0.04	0.00	27.99
2	0.87	0.00	46.26	0.00
3	1.30	0.00	0.87	0.01
4	1.51	0.02	0.00	27.13
5	1.71	0.00	4.84	0.00
6	2.63	0.78	1.67	0.00
7	2.63	12.47	0.05	0.03
8	2.82	0.18	0.01	6.44
9	2.90	0.00	4.90	0.01
10	3.80	0.00	4.07	0.00

From the static analysis of the finite element model, it can be found that the total mass of the landscape bridge is 357.74 t. According to the modal information in Table 1, the second order vibration mode (0.87 Hz) is sensitive to the lateral human-induced excitation and fluctuating wind, which can cause an excessive vibration when the resonance occurs. Although the vertical modal mass participation coefficient of the first order frequency (0.62 Hz) is large, the natural vibration frequency is too small to be excited by vertical human-induced excitation. Therefore, the vertical vibration should be focused on the fourth order vibration mode (1.51 Hz). The eighth mode (2.82 Hz) is likely to be excited by the second frequency component of vertical walking-induced excitation, which will be analyzed in the following as well.

Further, it also can be seen in Table 1 that, there is a slight coupling between the lateral vibration (Y direction) and the vertical vibration (Z direction) of the bridge, which is caused by the torsion. It is shown in Table 1 that for the third mode, seventh mode, eighth mode and ninth mode, Y-directional and Z-directional modal mass participation coefficients are 0.87% and 0.01%, 0.05% and 0.03%,

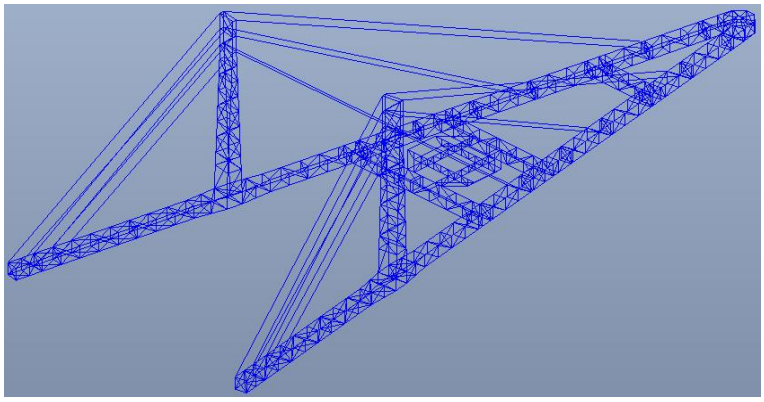

(a) Finite element model

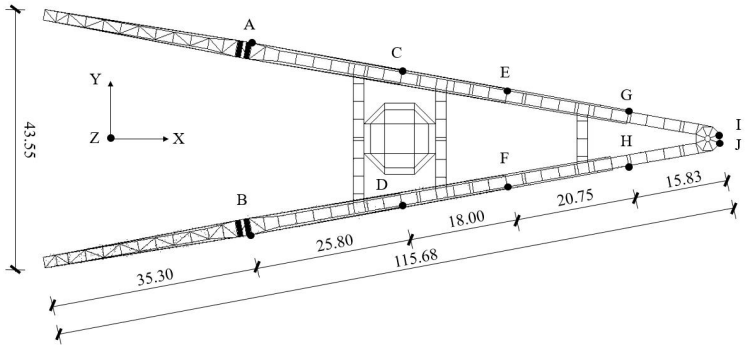

(b) Planform and measuring points (m)

Fig. 3 Cantilever cable-stayed landscape bridge

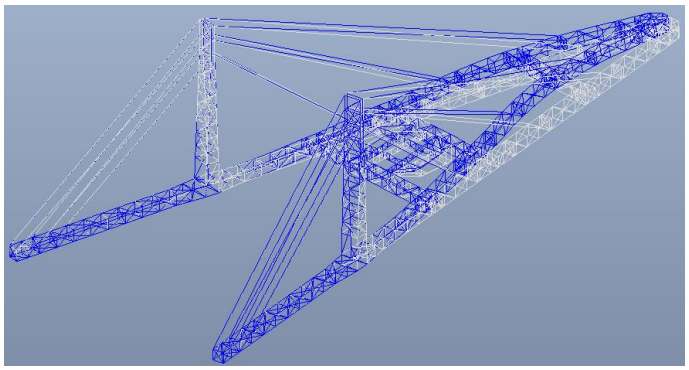

(a) The second order lateral mode (0.87 Hz)

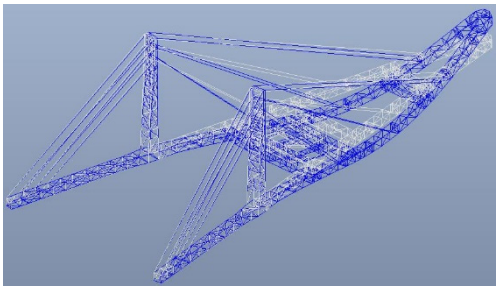

(b) The fourth order vertical mode (1.51 Hz)

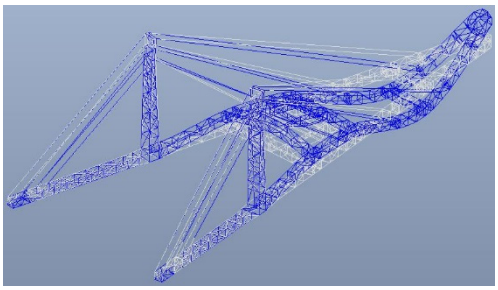

(c) The eighth order vertical mode (2.82 Hz)

Fig. 4 Susceptible modal shapes of the cable-stayed landscape bridge

0.01% and 6.44%, 4.90% and 0.01% respectively, which means that when the bridge has a lateral displacement in the Y direction, it also has a vertical displacement in the Z direction, which is caused by its torsion around the X axis. Therefore, it can be predicted that under lateral wind-induced excitation, a vertical vibration can also be measured because of the torsion. Concerned three modal shapes mentioned in the previous paragraph are illustrated in Fig. 4.

The eighth order vertical mode (2.82 Hz) in Fig. 4(c) and Table 1 includes lateral and vertical vibrations which are caused by torsion. The dominant frequency of the lateral pedestrian-induced load is half that of the vertical one. For vertical human-induced excitation, the center of mass (CM) of a pedestrian can complete a cycle of motion in vertical when the pedestrian only completes the left foot or the right foot forward. However, for lateral human-induced excitation, the pedestrian must complete both the left foot and right foot forward, then its CM in lateral can complete a cycle of movement. Therefore, the frequency of vertical human-induced excitation is twice that of lateral excitation. Therefore, in the following finite element analysis, three vertical pedestrian-induced excitations of 1.41 Hz (for the eighth order vertical mode), 1.51 Hz (for the fourth order vertical mode) and 1.74 Hz (for the second order lateral mode) are selected, together with the combined lateral pedestrian-induced excitation generated by them.

3.2 Retuning simulation of the MAP-TMD-TLD

According to modal shapes in Fig. 4, the MAP-TMD-TLD system is designed. Two AP-TMD-TLDs are implemented at the point E in Fig. 3(b), while one AP-TMD part is focused on the fourth order vertical mode (1.51 Hz), and the other is focused on the eighth order vertical mode (2.82 Hz). Their AP-TLD parts are both focused on the second order lateral mode (0.87 Hz). The same system as point E with two different AP-TMD-TLDs is also arranged at the point F, I, and J respectively. Therefore, the MAP-TMD-TLD system consists of eight AP-TMD-TLDs distributed at four points. Further, in real engineering, the four AP-TMD-TLDs at the location of measuring point I and J can be merged into one AP-TLD (for the lateral mode) with two AP-TMDs (for the two different vertical modes respectively) on it.

The total AP-TMD modal mass ratio for the fourth order vertical mode is about 4%, which is about 4.5% for the eighth order vertical mode. The total AP-TLD modal mass ratio for the second order lateral mode is about 3%. For comparison, initial parameters of the MAP-TMD-TLD system are set to be mistuned. The retuning function of the MAP-TMD-TLD system is verified in this section. Detailed parameters about the MAP-TMD-TLD system before and after the retuning operation are listed in Tables 2 and 3 respectively.

Under three-dimensional ambient excitation, which is simulated as the Gaussian white noise, the frequency retuning of the MAP-TMD-TLD system is carried out. Take the measuring point E and I for example, their time-frequency distributions through WT are illustrated in Fig. 5. It should be noted that the color bar in the figure means the power spectral density (PSD) of the signal.

In Fig. 5, the red line is the caught dominant frequency under ambient excitation for each time segment. The finial identified frequency is the mean of them. Then, the AP-TMD-TLD can retune its vertical and lateral frequencies both through varying the liquid level in the upper tank and bottom tank. After the above frequency retuning

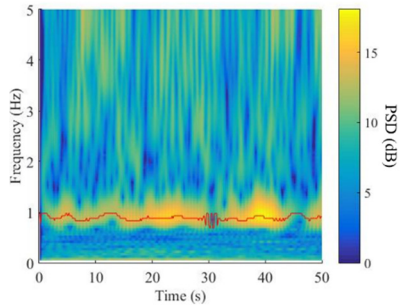

(a) Second order lateral frequency of point E

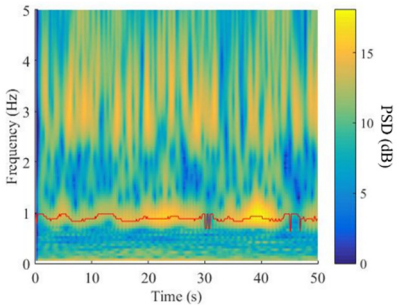

(b) Second order lateral frequency of point I

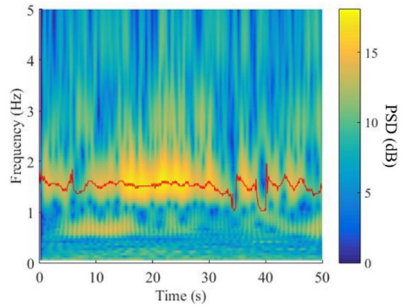

(c) Fourth order vertical frequency of point E

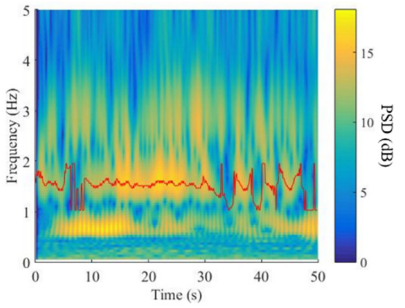

(d) Fourth order vertical frequency of point I

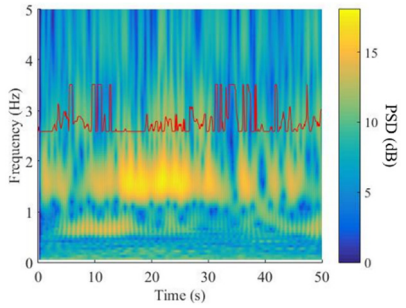

(e) Eighth order vertical frequency of point E

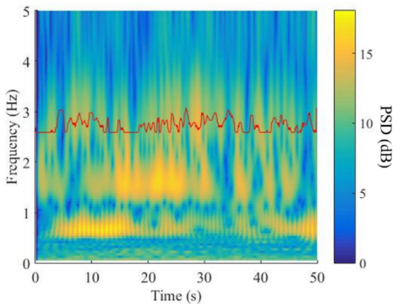

(f) Eighth order vertical frequency of point I

Fig. 5 Frequency retuning of the MAP-TMD-TLD system through WT

operation, it becomes a new MAP-TMD-TLD system with a reasonable frequency distribution. For comparison, retuned results are shown in Tables 2 and 3 respectively as well.

According to each modal mass ratio μ introduced in this section, the damping ratio ζ_{opt} is optimized based on Eq. (2) (Den 1985).

$$\zeta_{opt} = \sqrt{\frac{3\mu}{8(1+\mu)}} \tag{2}$$

Note that damping of the AP-TMD part is proposed by the vertical relative motion between the iron bar and silicone oil in the container, therefore, before and after the

Table 2 Parameters of AP-TMDs

No	Parameter	Mass (kg)	Frequency (Hz)	Damping ratio (%)	Stiffness (kN/m)	Damping coefficient (N•s/m)
1	Mistuned TMD - E - Fourth mode	1000	1.66	12.01	109.39	2512.24
2	Mistuned TMD - E - Eighth mode	260	3.10	12.73	98.93	1291.25
3	Mistuned TMD - I - Fourth mode	1000	1.66	12.01	109.39	2512.24
4	Mistuned TMD - I - Eighth mode	260	3.10	12.73	98.93	1291.25
5	Retuned TMD - E - Fourth mode	1220.25	1.51	10.87	109.39	2512.24
6	Retuned TMD - E - Eighth mode	323.13	2.78	11.42	98.93	1291.25
7	Retuned TMD - I - Fourth mode	1228.06	1.50	10.84	109.39	2512.24
8	Retuned TMD - I - Eighth mode	335.35	2.73	11.21	98.93	1291.25

Table 3 Parameters of AP-TLDs

No	Parameter	Mass (kg)	Frequency (Hz)	Liquid level (cm)
1	Mistuned TLD - E - Second mode	1005.60	0.96	33.52
2	Mistuned TLD - E - Second mode	251.40	0.96	33.52
3	Mistuned TLD - I - Second mode	1005.60	0.96	33.52
4	Mistuned TLD - I - Second mode	251.40	0.96	33.52
5	Retuned TLD - E - Second mode	716.40	0.89	23.88
6	Retuned TLD - E - Second mode	179.10	0.89	23.88
7	Retuned TLD - I - Second mode	716.40	0.89	23.88
8	Retuned TLD - I - Second mode	179.10	0.89	23.88

retuning operation, it is assumed that the damping coefficient is the same. The damping of the AP-TLD part is provided by the liquid itself and additional details.

It is shown in Table 2 that because of the location, there is a slight difference between the identification result of point E and I. However, they are similar generally and are close to the target modal frequency which are 1.51 Hz and 2.82 Hz respectively in Fig. 4. As for the two kinds of AP-TLD parts in Table 3, the length of them is both 75 cm, while the width of the larger one and smaller one is 400 cm and 100 cm respectively, whose retuned frequency is both 0.89 Hz and almost the same as the target structural lateral frequency (0.87 Hz), which shows a high identification accuracy.

4. Human-induced vibration control

In this section, human-induced vibration control is proposed, and structural responses are compared. The bi-directional vertical and lateral compound walking-induced excitation is simulated according to Wang and Chen (2017). The Fourier series based periodic walking-induced excitation is used, while the first three orders' frequency components are considered for the vertical load, and the first five orders' frequency components are considered for the lateral load.

In the finite element model, 20 pedestrians are evenly arranged along the walkway from the point A to I, each with a body weight of 700 N, and the same as the walkway from the point B to J in Fig. 3. A modal damping ratio of 1% is set for the steel cable-stayed landscape bridge.

Vertical and lateral structural responses comparisons are proposed in section 4.1 and 4.2 respectively.

4.1 Vertical response

Three vertical walking-induced excitations of 1.41 Hz (for the eighth order vertical mode), 1.51 Hz (for the fourth order vertical mode) and 1.74 Hz (for the second order lateral mode) are considered in this section. The time history and Fourier spectrum of the 1.51 Hz vertical walking-induced excitation are presented in Fig. 6.

Three typical measuring points along the walkway are selected for comparison, which are point C, E and I respectively. The maximum and root mean square (RMS) responses are both considered. Response comparison of the measuring point E under 1.51 Hz vertical walking-induced excitation and the measuring point I under 1.41 Hz vertical walking-induced excitation are shown in Figs. 7 and 8 respectively, while results are summarized in Table 4. In each "Reduction" part in the following tables, the first line means the vibration reduction of retuned TMD/TLD compared to the without control case, while the second line means the vibration reduction of retuned TMD/TLD compared to the mistuned TMD/TLD.

In Fig. 7, the structural fourth order vertical mode (1.51 Hz) is excited, though the mistuned TMD (1.66 Hz) can control the resonant response, the retuned TMD (1.51 Hz) performs better. In Fig. 8, the 1.41 Hz walking-induced excitation excites the structural fourth order vertical mode (1.51 Hz). It is obvious that the mistuned TMD (3.10 Hz) will amplify the structural response to a great degree, while the retuned TMD (2.73 Hz) can control it significantly.

It also can be seen in Table 4 that under the 1.74 Hz non-resonant excitation, the structural response is significantly smaller than the other two resonant cases. However, both mistuned TMD and retuned TMD will have a negative effect at this case, while the response is still

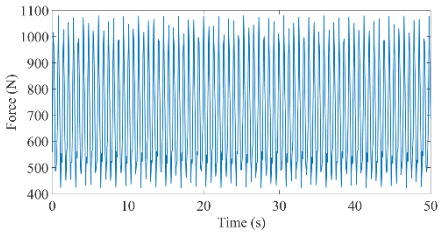

(a) Time history

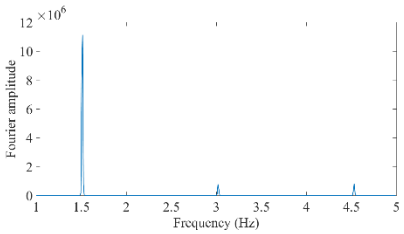

(b) Fourier spectrum

Fig. 6 1.51 Hz vertical walking-induced excitation

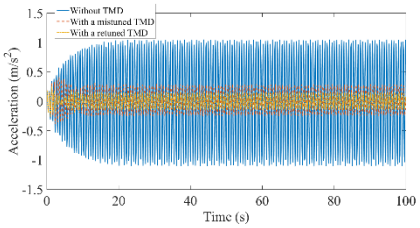

(a) Time history

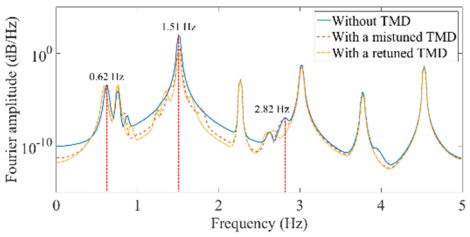

(b) Fourier spectrum

Fig. 7 Response comparison of the point E under 1.51 Hz vertical walking-induced excitation

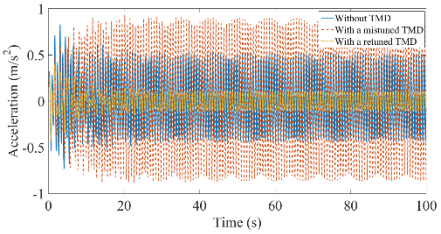

(a) Time history

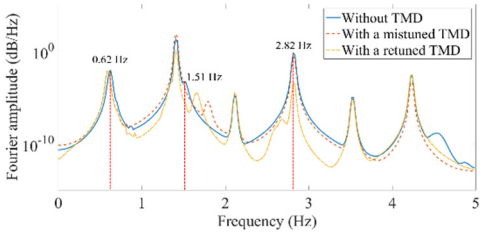

(b) Fourier spectrum

Fig. 8 Response comparison of the point I under 1.41 Hz vertical walking-induced excitation

Table 4 Control effect comparison of vertical human-induced vibration

Case	Maximum			RMS		
Vertical frequency (Hz)	1.41	1.51	1.74	1.41	1.51	1.74
Point C						
Without control (m/s^2)	0.2294	0.7418	0.1334	0.1300	0.5025	0.0902
Mistuned TMD (m/s^2)	0.5357	0.1623	0.0775	0.3736	0.1009	0.0466
Retuned TMD (m/s^2)	0.1295	0.0837	0.1928	0.0818	0.0497	0.1226
Reduction (%)	43.55	88.72	-44.53	37.08	90.11	-35.92
	75.83	48.43	-148.77	78.10	50.74	-163.09
Point E						
Without control (m/s^2)	0.3010	1.1087	0.2432	0.1943	0.7708	0.1410
Mistuned TMD (m/s^2)	0.9037	0.3174	0.1432	0.6294	0.1793	0.0761
Retuned TMD (m/s^2)	0.2683	0.1740	0.3013	0.1562	0.0986	0.1815
Reduction (%)	10.86	84.31	-23.89	19.61	87.21	-28.72
	70.31	45.18	-110.41	75.18	45.01	-138.50
Point I						
Without control (m/s^2)	0.5190	1.4035	0.1164	0.3290	0.9605	0.0837
Mistuned TMD (m/s^2)	0.9294	0.2434	0.2914	0.6146	0.1024	0.1336
Retuned TMD (m/s^2)	0.1716	0.2551	0.2860	0.0776	0.1058	0.1568
Reduction (%)	66.94	81.82	-145.70	76.41	88.98	-87.34
	81.54	-4.81	1.85	87.37	-3.32	-17.37

small relatively and the negative effect can be ignored. Further, compared to the other two points, the response of the point I is the maximum, which is located at the cantilever end of the bridge.

The structure has the maximum dynamic response in resonance, and the dynamic vibration absorber with well-tuned frequency has the best control effect in this case. When the excitation frequency deviates from the resonant frequency of the structure, the dynamic response decreases significantly, and the control effect of the absorber will also decrease, and even have a slight negative effect of amplifying the response. The numerical simulation results in this section also verify this point. From the whole frequency band, the absorber with well-tuned frequency has excellent control effect on the maximum response of the structure, and it is also better than the mistuned absorber.

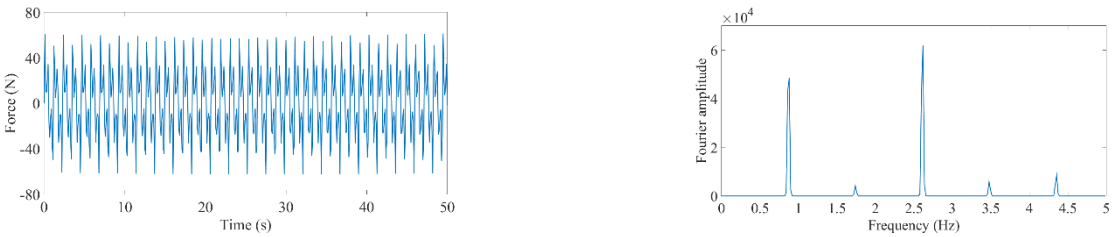

(a) Time history (b) Fourier spectrum

Fig. 9 0.87 Hz lateral walking-induced excitation

(a) Time history (b) Fourier spectrum

Fig. 10 Response comparison of the point E under 0.87 Hz lateral walking-induced excitation

Table 5 Control effect comparison of lateral human-induced vibration

Case	Maximum			RMS		
Lateral frequency (Hz)	0.71	0.76	0.87	0.71	0.76	0.87
Point C						
Without control (m/s^2)	0.0123	0.0260	0.0802	0.0068	0.0128	0.0501
Mistuned TLD (m/s^2)	0.0155	0.0149	0.0376	0.0073	0.0083	0.0173
Retuned TLD (m/s^2)	0.0104	0.0198	0.0216	0.0057	0.0095	0.0095
Reduction (%)	15.45	23.85	73.07	16.18	25.78	81.04
	32.90	-32.89	42.55	21.92	-14.46	45.09
Point E						
Without control (m/s^2)	0.0330	0.0380	0.1691	0.0134	0.0163	0.1114
Mistuned TLD (m/s^2)	0.0252	0.0339	0.0714	0.0122	0.0181	0.0346
Retuned TLD (m/s^2)	0.0245	0.0414	0.0314	0.0123	0.0213	0.0152
Reduction (%)	25.76	-8.95	81.43	8.21	-30.67	86.36
	2.78	-22.12	56.02	-0.82	-17.68	56.07
Point I						
Without control (m/s^2)	0.0213	0.0177	0.0703	0.0091	0.0094	0.0498
Mistuned TLD (m/s^2)	0.0140	0.0148	0.0379	0.0061	0.0079	0.0169
Retuned TLD (m/s^2)	0.0096	0.0210	0.0160	0.0051	0.0094	0.0069
Reduction (%)	54.93	-18.64	77.24	43.96	0.00	86.14
	31.43	-41.89	57.78	16.39	-18.99	59.17

Therefore, the negative effect of a slightly amplified response in the non-resonant segment is negligible, because the response of the structure itself is much smaller than in resonance.

The AP-TMD-TLD studied in this paper aims to identify and retune to the modal frequency of the structure. In future research, a semi-active MTMD-TLD system which can adjust its frequency to the instantaneous vibration frequency in real time will be meaningful.

4.2 Lateral response

Lateral responses are compared in this section. The time history and Fourier spectrum of the 0.87 Hz lateral walking-induced excitation, which is combined with the 1.74 Hz vertical excitation are illustrated in Fig. 9.

Response comparison of the measuring point E under 0.87 Hz lateral walking-induced excitation is proposed in Fig. 10, and detailed results are presented in Table 5.

In Fig. 10, the structural second order vibration mode (0.87 Hz) is excited, though the mistuned TLD (0.96 Hz) has a positive control effect, the retuned TLD (0.89 Hz) performs much better. From Table 5, the maximum response does not occur in the point I which is located at the cantilever end of the bridge, but occurs in the point E, which is consistent with the modal shape as shown in Fig. 4(a). Besides, the 0.71 Hz and 0.76 Hz lateral walking-induced excitations are both non-resonant, and their responses are therefore much smaller than the resonant 0.87 Hz case. Under the 0.71 Hz excitation, the retuned TLD also has the best control effect. However, it has a negative effect for the 0.76 Hz excitation. Considering the structural response and negative effect are both small relatively, it can be ignored certainly.

From this section, it can be found that the MAP-TMD-TLD system can control both walking-induced vertical and lateral vibrations effectively.

5. Wind-induced vibration control

Wind-induced vibration control effect is investigated in this section. According to the design requirements, the basic wind pressure is 0.3 KPa, therefore, the average wind speed at the height of 10 m under fluctuating wind excitation is 21.9 m/s. The fluctuating wind in this section is simulated according to the auto-regressive (AR) model (Sun *et al*. 2019, Wang *et al*. 2021b).

As can be seen from the modal shape as presented in Fig. 4, the twin towers and their left sides of the landscape bridge have almost no modal displacement. Therefore, only the walkway from the point A to I is excited by the fluctuating wind. The total area of the walkway from the point A to I section is 116.19 m^2, and the fluctuating wind is equivalent to 10 concentrated forces evenly distributed along the walkway.

The simulated concentrated force of the fluctuating wind is presented in Fig. 11.

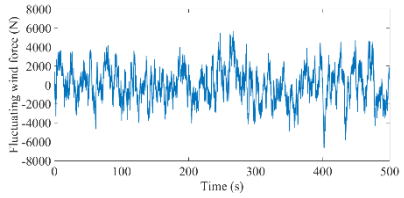

Fig. 11 Fluctuating wind force generated through the AR method

5.1 Lateral response

Lateral responses under wind-induced excitation are proposed in this section. Response comparison of the measuring point E is shown in Fig. 12, while numerical results are compared in Table 6.

It can be found in Fig. 12 and Table 6 that, under wind-induced excitation, the retuned TLD has the best control effect for the whole three measuring points, and both for maximum and RMS responses. Meanwhile, it also can be seen that the maximum response occurs in the point E but not the point I which is located at the cantilever end of the bridge, which is consistent with the results in section 4.2.

5.2 Vertical response

Because of the slight torsional response as shown in Table 1 and Fig. 4, it is found that though only under the lateral wind-induced excitation, vertical vibrations are caused as well. Control effect comparison of vertical wind-induced vibration is proposed in Table 7.

It can be seen in Table 7 that generally, the retuned TMD has a better control effect than the mistuned TMD before the retuning operation especially in the RMS response, and can control the wind-induced vertical vibration effectively. As for human-induced vertical vibration in section 4.1, the maximum response occurs in the point I. However, the maximum response occurs in

Table 6 Control effect comparison of lateral wind-induced vibration

Case	Maximum			RMS		
Point	C	E	I	C	E	I
Without control (m/s^2)	0.0839	0.3259	0.0978	0.0315	0.0926	0.0331
Mistuned TLD (m/s^2)	0.0736	0.1643	0.0859	0.0267	0.0596	0.0273
Retuned TLD (m/s^2)	0.0710	0.1524	0.0640	0.0229	0.0490	0.0227
Reduction (%)	15.38	53.24	34.56	27.30	47.08	31.42
	3.53	7.24	25.49	14.23	17.79	16.85

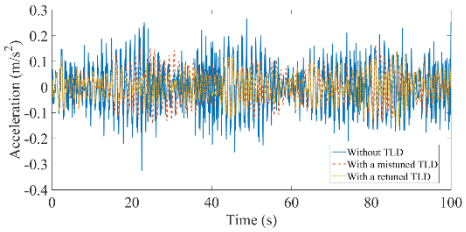

(a) Time history

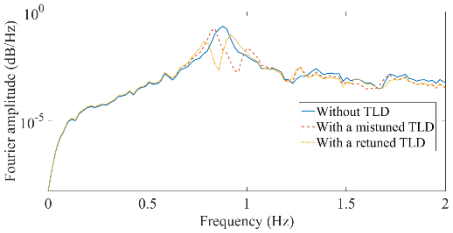

(b) Fourier spectrum

Fig. 12 Lateral response comparison of the measuring point E under wind-induced excitation

Table 7 Control effect comparison of vertical wind-induced vibration

Case	Maximum			RMS		
Point	C	E	I	C	E	I
Without control (m/s^2)	0.0440	0.0924	0.0247	0.0120	0.0279	0.0066
Mistuned TLD (m/s^2)	0.0299	0.0680	0.0159	0.0104	0.0245	0.0055
Retuned TLD (m/s^2)	0.0295	0.0705	0.0158	0.0088	0.0208	0.0047
Reduction (%)	32.95	23.70	36.03	26.67	25.45	28.79
	1.34	-3.68	0.63	15.38	15.10	14.55

the point E in this section, which is consistent with results shown in section 5.1.

From this section, it can be concluded that the MAP-TMD-TLD system has a satisfactory serviceability improvement performance for wind-induced lateral and vertical vibrations.

6. Human- and wind-induced compound vibration control

In this section, for a more complex case, human- and wind-induced vertical and lateral bi-directional compound vibration is considered, and structural responses are compared.

6.1 Vertical compound response

Vertical response comparison of the measuring point E under 1.51 Hz vertical walking and wind-induced compound excitation, and the measuring point I under 1.41 Hz vertical walking and wind-induced compound excitation are illustrated in Figs. 13 and 14 respectively, while results are listed in Table 8.

From Figs. 13, 14 and Table 8 in this section, it can be known that the tendency is the same as section 4.1, which means that the vertical walking-induced excitation is dominant in this compound excitation. Besides, compare this section with section 4.1 and 5.2, it can be found that the structural response in this section is slightly less than the sum of section 4.1 and 5.2. The maximum response occurs in the point I which is located at the cantilever end of the bridge.

Generally, the retuned MAP-TMD-TLD system has an excellent control effect in vertical walking and wind-induced compound vibration.

6.2 Lateral compound response

Lateral response comparison of the measuring point E under 0.87 Hz lateral walking and wind-induced excitation is shown in Fig. 15, while numerical results can be seen in Table 9.

From Fig. 15 and Table 9 in this section, it can be found that the tendency is between section 4.2 and 5.1, and generally, the wind-induced excitation is dominant in this lateral compound excitation. Besides, compare this section with section 4.2 and 5.1, it also can be known that the structural response in this section is slightly less than the sum of section 4.2 and 5.1. The maximum response occurs in the point E, which is consistent with the modal shape as shown in Fig. 4(a).

In section 4.2, under the 0.76 Hz lateral non-resonant excitation, the retuned TLD has a negative effect. However,

(a) Time history (b) Fourier spectrum

Fig. 13 Response comparison of the measuring point E under 1.51 Hz vertical walking and wind-induced compound excitation

(a) Time history (b) Fourier spectrum

Fig. 14 Response comparison of the measuring point I under 1.41 Hz vertical walking and wind-induced compound excitation

Table 8 Control effect comparison of vertical walking and wind-induced compound excitation

Case	Maximum			RMS		
Vertical frequency (Hz)	1.41	1.51	1.74	1.41	1.51	1.74
Point C						
Without control (m/s^2)	0.2519	0.7675	0.1555	0.1315	0.5023	0.0908
Mistuned TMD (m/s^2)	0.5528	0.1785	0.0990	0.3740	0.1010	0.0478
Retuned TMD (m/s^2)	0.1454	0.0921	0.2074	0.0819	0.0500	0.1231
Reduction (%)	42.28	88.00	-33.38	37.72	90.05	-35.57
	73.70	48.40	-109.49	78.10	50.50	-157.53
Point E						
Without control (m/s^2)	0.3847	1.1725	0.3129	0.1988	0.7706	0.1434
Mistuned TMD (m/s^2)	0.9478	0.3511	0.1824	0.6303	0.1800	0.0802
Retuned TMD (m/s^2)	0.2974	0.2020	0.3340	0.1565	0.1001	0.1830
Reduction (%)	22.69	82.77	-6.74	21.28	87.01	-27.62
	68.62	42.47	-83.11	75.17	44.39	-128.18
Point I						
Without control (m/s^2)	0.6218	1.4264	0.2567	0.3279	0.9611	0.0833
Mistuned TMD (m/s^2)	0.9313	0.2377	0.2941	0.6144	0.1028	0.1337
Retuned TMD (m/s^2)	0.1738	0.2515	0.2876	0.0779	0.1060	0.1568
Reduction (%)	72.05	82.37	-12.04	76.24	88.97	-88.24
	81.34	-5.81	2.21	87.32	-3.11	-17.28

Table 9 Control effect comparison of lateral walking and wind-induced compound excitation

Case	Maximum			RMS		
Lateral frequency (Hz)	0.71	0.76	0.87	0.71	0.76	0.87
Point C						
Without control (m/s^2)	0.0955	0.1084	0.1553	0.0322	0.0339	0.0549
Mistuned TMD (m/s^2)	0.0768	0.0833	0.0869	0.0275	0.0279	0.0311
Retuned TMD (m/s^2)	0.0807	0.0700	0.0760	0.0232	0.0248	0.0246
Reduction (%)	15.50	35.42	51.06	27.95	26.84	55.19
	-5.08	15.97	12.54	15.64	11.11	20.90
Point E						
Without control (m/s^2)	0.3112	0.3185	0.4588	0.0931	0.0939	0.1359
Mistuned TMD (m/s^2)	0.1524	0.1741	0.1860	0.0603	0.0623	0.0667
Retuned TMD (m/s^2)	0.1711	0.1471	0.1550	0.0497	0.0531	0.0507
Reduction (%)	45.02	53.81	66.22	46.62	43.45	62.69
	-12.27	15.51	16.67	17.58	14.77	23.99
Point I						
Without control (m/s^2)	0.1017	0.0983	0.1510	0.0343	0.0343	0.0555
Mistuned TMD (m/s^2)	0.0871	0.0802	0.0942	0.0278	0.0284	0.0312
Retuned TMD (m/s^2)	0.0675	0.0681	0.0676	0.0229	0.0245	0.0236
Reduction (%)	33.63	30.72	55.23	33.24	28.57	57.48
	22.50	15.09	28.24	17.63	13.73	24.36

it has the best mitigation effect for the 0.76 Hz walking and wind-induced compound excitation in this section, because the wind-induced excitation is dominant in it.

From this section, it can be known that the retuned MAP-TMD-TLD system can control the human- and wind-induced vertical and lateral bi-directional compound

(a) Time history (b) Fourier spectrum

Fig. 15 Response comparison of the measuring point E under 0.87 Hz lateral walking and wind-induced compound excitation

vibration quite effectively.

7. Conclusions

To improve the structural serviceability against external excitations for slender structures and propose a smart electromechanical device that can simultaneously control vertical and lateral compound vibration, a combined adaptive-passive TMD-TLD (AP-TMD-TLD) system is proposed in this study. The vertical AP-TMD part on top of the vertical spring can retune itself through varying the level of liquid in the tank to adjust its mass, and the lateral AP-TLD part at the bottom of the vertical spring can retune itself by changing the level of liquid. For multimodal response control, the multiple AP-TMD-TLD (MAP-TMD-TLD) system is presented further. For each AP-TMD-TLD in the MAP-TMD-TLD system, it can identify the structural vertical and lateral modal frequencies through the wavelet-transform (WT) based algorithm and retune its vertical and lateral natural frequencies both through adjusting the level of liquid in the AP-TMD part and AP-TLD part respectively.

A steel cantilever cable-stayed landscape bridge which is sensitive to both human-induced vertical/lateral vibration and wind-induced lateral vibration is presented as a case study. For comparison, initial parameters of the MAP-TMD-TLD system are set to be mistuned.

From finite element analysis proposed in section 3~6, main conclusions can be summarized as following:

(1) The MAP-TMD-TLD system can identify structural target modal frequencies in selected locations with a high accuracy, and then retune itself to a new system with a reasonable frequency distribution;

(2) As for walking-induced vibrations, the mistuned TMD may amplify the structural response to a great degree, while the retuned TMD can control it significantly. Generally, the MAP-TMD-TLD system can control both walking-induced vertical and lateral multimodal responses effectively;

(3) Because of the slight torsional response, vertical vibrations can be excited under the lateral wind-induced excitation. The MAP-TMD-TLD system has a satisfactory serviceability improvement performance for wind-induced lateral and vertical vibration. It has the best control effect for the whole three measuring points, and both for maximum and RMS responses;

(4) Generally, the retuned MAP-TMD-TLD system can control the human- and wind-induced vertical and lateral bi-directional compound multimodal responses quite effectively and improve the structural serviceability significantly.

Acknowledgments

The authors are grateful for the financial support received from the National Natural Science Foundation of China (Grant no. 52308526, 52025083), National Key Research and Development Program of China (Grant no. 2022YFF0608903), and this study is also sponsored by Shanghai Pujiang Program (22PJ1413600), supported by the Fundamental Research Funds for the Central Universities (22120220573, 0200121005/174), and Scientific Research Fund of Institute of Engineering Mechanics, China Earthquake Administration (Grant No. 2023D02).

References

Acosta, J., Bojórquez, E., Bojórquez, J., Reyes-Salazar, A., Payan, O., Barraza, M. and Serrano, J. (2022), "Control of peak floor accelerations of buildings under wind loads using tuned mass damper", *Struct. Eng. Mech., Int. J.*, **81**(1), 1-9. https://doi.org/10.12989/sem.2022.81.1.001

Bocian, M., Macdonald, J.H., Burn, J.F. and Redmill, D. (2015), "Experimental identification of the behaviour of and lateral forces from freely-walking pedestrians on laterally oscillating structures in a virtual reality environment", *Eng. Struct.*, **105**, 62-76. https://doi.org/10.1016/j.engstruct.2015.09.043

Brownjohn, J.M.W., Chen, J., Bocian, M., Racic, V. and Shahabpoor, E. (2018), "Using inertial measurement units to identify medio-lateral ground reaction forces due to walking and swaying", *J. Sound Vib.*, **426**, 90-110. https://doi.org/10.1016/j.jsv.2018.04.019

Cao, L. and Chen, Y. (2020), "A simplified method for determining the acceleration amplitudes of long-span floor system under walking/running loads", *Struct. Eng. Mech., Int. J.*, **75**(3), 377-387. https://doi.org/10.12989/sem.2020.75.3.377

Casado, C.M., Díaz, I.M., de Sebastián, J., Poncela, A.V. and Lorenzana, A. (2013), "Implementation of passive and active vibration control on an in-service footbridge", *Struct. Contr. Health Monit.*, **20**(1), 70-87. https://doi.org/10.1002/stc.471

Den, H. (1985), *Mechanical Vibrations*, McGraw-Hill/Dover: New York, NY, USA.

Ferreira, F. and Simões, L. (2019), "Least cost design of curved cable-stayed footbridges with control devices", *Structures*, **19**, 68-83. https://doi.org/10.1016/j.istruc.2018.12.004

Ferreira, F., Moutinho, C., Cunha, Á. and Caetano, E. (2019), "Use

of semi-active tuned mass dampers to control footbridges subjected to synchronous lateral excitation", *J. Sound Vib.*, **446**, 176-194. https://doi.org/10.1016/j.jsv.2019.01.026

Hoa, T.N., Khatir, S., De Roeck, G., Long, N.N., Thanh, B.T. and Wahab, M.A. (2020), "An efficient approach for model updating of a large-scale cable-stayed bridge using ambient vibration measurements combined with a hybrid metaheuristic search algorithm", *Smart Struct. Syst., Int. J.*, **25**(4), 487-499. https://doi.org/10.12989/sss.2020.25.4.487

Ingólfsson, E.T., Georgakis, C.T. and Jönsson, J. (2012), "Pedestrian-induced lateral vibrations of footbridges: a literature review", *Eng. Struct.*, **45**(15), 21-52. https://doi.org/10.1016/j.engstruct.2012.05.038

Jiménez-Alonso, J. and Sáez, A. (2018), "Motion-based design of TMD for vibrating footbridges under uncertainty conditions", *Smart Struct. Syst., Int. J.*, **21**(6), 727-740. https://doi.org/10.12989/sss.2018.21.6.727

Jiménez-Alonso, J.F., Sáez, A., Caetano, E. and Cunha, Á. (2019), "Lateral crowd-structure interaction model to analyse the change of the modal properties of footbridges", *Struct. Contr. Health Monit.*, **26**(6), e2356. https://doi.org/10.1002/stc.2356

Khazaali, M., Ma, L., Rokneddin, K., Mazzotti, M. and Bocchini, P. (2024), "A robust protocol to compute wind load coefficients of telecommunication towers and antennas using numerical simulation for risk and resilience assessment", *Resilient Cities Struct.*, **3**, 66-83. https://doi.org/10.1016/j.rcns.2024.02.001

Kontoni, D. and Farghaly, A. (2019), "Mitigation of the seismic response of a cable-stayed bridge with soil-structure-interaction effect using tuned mass dampers", *Struct. Eng. Mech., Int. J.*, **69**(6), 699-712. https://doi.org/10.12989/sem.2019.69.6.699

Lalonde, E.R., Dai, K., Bitsuamlak, G., Lu, W. and Zhao, Z. (2020), "Comparison of semi-active and passive tuned mass damper systems for vibration control of a wind turbine", *Wind Struct., Int. J.*, **30**(6), 663-678. https://doi.org/10.12989/was.2020.30.6.663

Larsen, A. and Larose, G. (2015), "Dynamic wind effects on suspension and cable-stayed bridges", *J. Sound Vib.*, **334**, 2-28. https://doi.org/10.1016/j.jsv.2014.06.009

Lazzari, P.M., Lazzari, B.M., Pacheco, A.R. and Gomes, R.R. (2019), "Numerical simulation of the constructive steps of a cable-stayed bridge using ANSYS", *Struct. Eng. Mech., Int. J.*, **69**(3), 269-281. https://doi.org/10.12989/sem.2019.69.3.269

Liu, M., Li, S. and Chen, Z. (2020a), "Mitigation of wind-induced responses of cylinder solar tower by a tiny eddy current tuned mass damper based on elastic wind tunnel tests", *Smart Struct. Syst., Int. J.*, **26**(5), 619-629. https://doi.org/10.12989/sss.2020.26.5.619

Liu, S., Lu, Z., Li, P., Ding, S. and Wan, F. (2020b), "Shaking table test and numerical simulation of eddy current tuned mass damper for structural seismic control considering soil-structure interaction", *Eng. Struct.*, **212**, 110531. https://doi.org/10.1016/j.engstruct.2020.110531

Moutinho, C., Cunha, Á., Caetano, E. and De Carvalho, J.M. (2018), "Vibration control of a slender footbridge using passive and semiactive tuned mass dampers", *Struct. Contr. Health Monit.*, **25**(9), e2208. https://doi.org/10.1002/stc.2208

Nagarajaiah, S. (2010), "Adaptive passive, semiactive, smart tuned mass dampers: identification and control using empirical mode decomposition, hilbert transform, and short-term fourier transform", *Struct. Contr. Health Monit.*, **16**(7-8), 800-841. https://doi.org/10.1002/stc.349

Nagarajaiah, S. and Sonmez, E. (2007), "Structures with semiactive variable stiffness single/multiple tuned mass dampers", *J. Struct. Eng.*, **133**(1), 67-77. https://doi.org/10.1061/(ASCE)0733-9445(2007)133:1(67)

Nagarajaiah, S. and Varadarajan, N. (2005), "Short time fourier transform algorithm for wind response control of buildings with variable stiffness TMD", *Eng. Struct.*, **27**(3), 431-441. https://doi.org/10.1016/j.engstruct.2004.10.015

Qian, C., Zhu, L., Zhu, Q., Ding, Q. and Yan, L. (2022), "Pattern and mechanism of wind-induced static instability of super-long-span cable-stayed bridge under large deformation", *J. Wind Eng. Ind. Aerod.*, **221**, 104910. https://doi.org/10.1016/j.jweia.2022.104910

Racic, V. and Brownjohn, J. (2012), "Mathematical modelling of random narrow band lateral excitation of footbridges due to pedestrians walking", *Comput. Struct.*, **90-91**, 116-130. https://doi.org/10.1016/j.compstruc.2011.10.002

Raeesi, A., Cheng, S. and Ting, D. (2019), "Application of a three-dimensional aeroelastic model to study the wind-induced response of bridge stay cables in unsteady wind conditions", *J. Sound Vib.*, **375**, 217-236. https://doi.org/10.1016/j.jsv.2016.04.019

Shad, H., Adnan, A., Behbahani, H.P. and Vafaei, M. (2016), "Efficiency of TLDs with bottom-mounted baffles in suppression of structural responses when subjected to harmonic excitations", *Struct. Eng. Mech., Int. J.*, **60**(1), 131-148. https://doi.org/10.12989/sem.2016.60.1.131

Shad, H., bin Adnan, A., Vafaei, M., Behbahani, H.P. and Oladimeji, A.M. (2018), "Experimental study on TLDs equipped with an upper mounted baffle", *Smart Struct. Syst., Int. J.*, **21**(1), 37-51. https://doi.org/10.12989/sss.2018.21.1.037

Spencer Jr, B.F. and Nagarajaiah, S. (2003), "State of the art of structural control", *J. Struct. Eng.*, **129**(7), 845-856. https://doi.org/10.1061/(ASCE)0733-9445(2003)129:7(845)

Sun, C. and Nagarajaiah, S. (2014), "Study on semi-active tuned mass damper with variable damping and stiffness under seismic excitations", *Struct. Contr. Health Monit.*, **21**(6), 890-906. https://doi.org/10.1002/stc.1620

Sun, C., Nagarajaiah, S. and Dick, A.J. (2014), "Family of smart tuned mass dampers with variable frequency under harmonic excitations and ground motions: closed-form evaluation", *Smart Struct. Syst., Int. J.*, **13**(2), 319-341. https://doi.org/10.12989/sss.2014.13.2.319

Sun, C., Jahangiri, V. and Sun, H. (2019), "Performance of a 3D pendulum tuned mass damper in offshore wind turbines under multiple hazards and system variations", *Smart Struct. Syst., Int. J.*, **24**(1), 53-65. https://doi.org/10.12989/sss.2019.24.1.053

Wang, J. and Chen, J. (2017), "A comparative study on different walking load models", *Struct. Eng. Mech., Int. J.*, **63**(6), 847-856. https://doi.org/10.12989/sem.2017.63.6.847

Wang, L., Shi, W., Zhang, Q. and Zhou, Y. (2020a), "Study on adaptive-passive multiple tuned mass damper with variable mass for a large-span floor structure", *Eng. Struct.*, **209**, 110010. https://doi.org/10.1016/j.engstruct.2019.110010

Wang, L., Shi, W., Zhou, Y. and Zhang, Q. (2020b), "Semi-active eddy current pendulum tuned mass damper with variable frequency and damping", *Smart Struct. Syst., Int. J.*, **25**(1), 65-80. https://doi.org/10.12989/sss.2020.25.1.065

Wang, X.C., Teng, Q., Duan, Y.F., Yun, C.B., Dong, S.L. and Lou, W.J. (2020c), "Optimal design of multiple tuned mass dampers for vibration control of a cable-supported roof", *Smart Struct. Syst., Int. J.*, **26**(5), 545-558. https://doi.org/10.12989/sss.2020.26.5.545

Wang, L., Nagarajaiah, S., Shi, W. and Zhou, Y. (2021a), "Semi-active control of walking-induced vibrations in bridges using adaptive tuned mass damper considering human-structure-interaction", *Eng. Struct.*, **244**, 112743. https://doi.org/10.1016/j.engstruct.2021.112743

Wang, M., Nagarajaiah, S. and Sun, F.F. (2021b), "Optimal design of supplemental negative stiffness damped outrigger system for high-rise buildings resisting multi-hazard of winds and earthquakes", *J. Wind Eng. Ind. Aerod.*, **218**, 104761. https://doi.org/10.1016/j.jweia.2021.104761

Wang, Y., Wang, L. and Shi, W. (2021c), "Two-dimensional air spring based semi-active TMD for vertical and lateral walking and wind-induced vibration control", *Struct. Eng. Mech., Int. J.*, **80**(4), 377-390. https://doi.org/10.12989/sem.2021.80.4.377

Wang, L., Nagarajaiah, S., Zhou, Y. and Shi, W. (2023), "Experimental study on adaptive-passive tuned mass damper with variable stiffness for vertical human-induced vibration control", *Eng. Struct.*, **280**, 115714. https://doi.org/10.1016/j.engstruct.2023.115714

Wang, L., Zhou, Y. and Shi, W. (2024), "Random crowd-induced vibration in footbridge and adaptive control using semi-active TMD including crowd-structure interaction", *Eng. Struct.*, **306**, 117839. https://doi.org/10.1016/j.engstruct.2024.117839

Xing, L., Gardoni, P. and Zhou, Y. (2022), "Kriging metamodels for the dynamic response of high-rise buildings with outrigger systems and fragility estimates for seismic and wind loads", *Resilient Cities Struct.*, **1**, 110-122. https://doi.org/10.1016/j.rcns.2022.04.003

Zahrai, S. and Kakouei, S. (2019), "Shaking table tests on a SDOF structure with cylindrical and rectangular TLDs having rotatable baffles", *Smart Struct. Syst., Int. J.*, **24**(3), 391-401. https://doi.org/10.12989/sss.2019.24.3.391

Zhu, Q., Hui, X., Du, Y. and Zhang, Q. (2019), "A full path assessment approach for vibration serviceability and vibration control of footbridges", *Struct. Eng. Mech., Int. J.*, **70**(6), 765-779. https://doi.org/10.12989/sem.2019.70.6.765

Zuo, H., Bi, K. and Hao, H. (2020), "Simultaneous out-of-plane and in-plane vibration mitigations of offshore monopile wind turbines by tuned mass dampers", *Smart Struct. Syst., Int. J.*, **26**(4), 435-449. https://doi.org/10.12989/sss.2020.26.4.435